ACS APPLIED ENERGY MATERIALS
Cite This: ACS Appl. Energy Mater. 2019, 2, 3860−3868
Article
www.acsaem.org

Unraveling the Li_2S Deposition Process on a Polished Graphite Cathode for Enhancing Discharge Capacity of Lithium−Sulfur Batteries

Chao Shen,[†,‡] Petru Andrei,[†,‡] and Jim P. Zheng*[,†,‡,§]

[†]Department of Electrical and Computer Engineering, Florida A&M University and Florida State University, Tallahassee, Florida 32310, United States

[‡]Aero-Propulsion, Mechatronics and Energy Center, Florida State University, Tallahassee, Florida 32310, United States

[§]Center for Advanced Power Systems, Florida State University, Tallahassee, Florida 32310, United States

Supporting Information

ABSTRACT: Solid deposition accounts for three-quarters of the theoretical capacity in lithium−sulfur (Li−S) batteries with liquid electrolyte. Despite extensive research efforts on cathode material synthesis, little knowledge has been gained so far in understanding and controlling the growth of solid discharge product in Li−S batteries. In this work, a polished graphite was used as a cathode to understand the growth mechanism of Li_2S. The SEM/EDS analysis of the discharged cathodes indicates that the Li_2S precipitate can grow over a micrometer in size and its morphology strongly depends on the depth of discharge (DODs) and discharge rate of the cell. In addition, the morphology evolution and the in situ electrochemical impedance spectra (EIS) show that the Li_2S follows a dissolution−precipitation mechanism during its deposition on the graphite surface. Finally, a mathematical model based on the multicomponent transport theory is developed and used to describe the nucleation and precipitation phenomena on the 2D surface and the EIS spectra at different DODs. The model confirms that the surface passivation of the cathode plays a major role during the discharge of the battery and offers a simple way to measure experimentally the surface coverage as a function of the DOD in Li−S batteries. This work highlights the importance of deferring cathode surface passivation in Li−S batteries and indicates the potential utilization of nonporous carbons as alternative sulfur hosts.

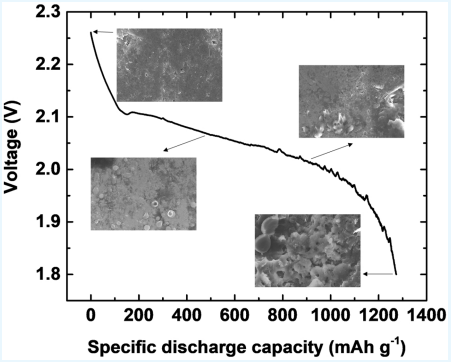

KEYWORDS: *Li_2S deposition, polished graphite, lithium sulfur batteries, surface coverage, modeling*

1. INTRODUCTION

Conventional lithium ion batteries (LIBs) have dominated the portable electronic devices market for more than 30 years.[1] However, as the energy density of LIBs approaches their theoretical limits, an alternative battery chemistry that will transform the current energy landscape is currently highly needed. Lithium−sulfur (Li−S) batteries, made of a sulfur cathode and a lithium anode, can provide a theoretical specific energy considerably higher than that of LIBs.[2,3] Both sulfur and lithium are light-weight elements with a theoretical specific capacity of 1672 and 3860 mAh g^{-1}, respectively. Considering an average voltage of 2.15 V, the theoretical specific energy is 2500 Wh kg^{-1} based on the mass of active materials. However, several significant technical challenges must be overcome to fully achieve the great potential of Li−S batteries. The insulating nature of sulfur and Li_2S limits the effective utilization of active material,[4,5] and the formation of intermediate lithium polysulfides (LiPS) in the electrolyte limits the battery capacities at low electrolyte/sulfur (E/S) ratios and participates in severe shuttle effects over long-term cycles;[6−8] additionally, the use of the lithium anode possesses some persistent issues to be solved such as dendrite formation and surface passivation.[9]

Ultimately, the most critical question to answer for Li−S batteries is whether their high theoretical energy density can be practically delivered. By analyzing the voltage profiles of Li−S batteries, one observes that three-quarters of the theoretical specific capacity (i.e., 1254 mAh g^{-1} out of 1672 mAh g^{-1}) comes from the lower plateau, which involves the process of Li_2S deposition (although Li_2S_2 has sometimes been suggested as another solid discharge product, there is no clear experimental evidence that this product is formed and is stable, and Li_2S_2 is more recognized as a transient species in recent publications[10]). Currently, the difference between the practical specific capacities of various reported Li−S batteries and their theoretical capacities is mainly attributed to the incomplete Li_2S deposition process.[11−15] The final discharge product Li_2S was shown experimentally as an insulating

Received: March 12, 2019
Accepted: May 8, 2019
Published: May 8, 2019

DOI: 10.1021/acsaem.9b00524
ACS Appl. Energy Mater. 2019, 2, 3860−3868

material that covers the active cathode surface during discharge and increases the charge-transfer resistance. It was measured that the stoichiometric Li_2S has an electronic resistivity higher than 10^{14} Ω cm, which causes the passivation of active surface area and decreases the practical specific capacity.[16,17] Moreover, the uncontrollable accumulation of insulating Li_2S poses a significant challenge for the stable cycling of Li−S batteries especially under lean electrolyte conditions.[18−20]

Unfortunately, little knowledge has been gained so far to understand and control the growth of solid discharge product despite the extensive research efforts on cathode material synthesis. Experimentally, the morphology of Li_2S is found to be highly dependent on the discharge rate and cathode configuration.[21−23] On the basis of ex situ scanning electron microscopy (SEM) imaging, Fan et al.[22] and Ren et al.[23] observed larger Li_2S particles at low discharge rates and a thin, uniform deposition layer at high rates. Moreover, some redox mediators have been reported to facilitate the film growing along the thickness direction instead of lateral growth to produce sub-micron-sized and porous 3D deposits.[24,25] Recently, large Li_2S particles with the size of over 1 μm were observed in low-surface-area cathode materials.[26,27] As pointed out by a number of research groups, the morphology of the Li_2S deposit can be controlled by optimizing the solvent,[28] lithium salt,[29,30] and electrode[31] in order to improve the discharge capacity of Li−S batteries.

In addition to the experimental investigation, there are also some modeling studies that study the growth mechanism of Li_2S. Using density function theory simulations, Liu et al.[32] developed an interfacial model for surface passivation on the carbon cathode and defined three stages of Li_2S film growth. Ren et al.[23] and Andrei et al.[33] proposed rate-dependent models for Li_2S deposition, which agree well with the experimental SEM observations. However, Zhang et al.[34] found that the cathode surface covered by Li_2S was simply proportional to the state-of-charge and was not rate-dependent.

Here we use a near-2D flat polished graphite as the standard cathode material in an effort to obtain a better understanding of the growth mechanism of Li_2S. We conducted combined experimental and theoretical investigations of the precipitation process of Li_2S on the carbon surface. Our results strongly support that the growth of Li_2S is a dissolution−precipitation process and the morphology of the final Li_2S particles depends on the DOD and discharge rate. This work is expected to provide insight for developing efficient strategies to address the cathode surface passivation issue in Li−S batteries for improving the practical specific capacity of Li−S batteries.

2. EXPERIMENTAL SECTION

Lithium sulfide was purchased from Alfa Aesar. Sulfur, bis-(trifluoromethane)sulfonimide (LiTFSI), the lithium nitrate powders, and the DME and DOL solvent were purchased from Sigma-Aldrich. Inside an argon-filled glovebox (MBraun), Li_2S_4 catholyte was prepared by weighing Li_2S and S in a stoichiometric ratio of 1:3 and stirring them together in the DME/DOL (1:1 v/v) solution at 45 °C until no precipitates were left. LiTFSI and $LiNO_3$ were also added in the solution, forming a Li_2S_4 catholyte solution with a composition of 0.5 M Li_2S_4, 0.5 M LiTFSI, and 0.1 M $LiNO_3$ in DME/DOL (1:1 v/v).

The graphite cathode (IG-56) was purchased from Toyo Tanso, Japan. The graphite, polished on one side, had a surface roughness Ra of 0.75 and a thickness of 1 mm. The Li−S cells were assembled using graphite as cathode, lithium metal (MTI) as anode, and Li_2S_4 catholyte as electrolyte in CR2032-type coin batteries. The polished graphite surface was placed toward the separator to ensure that the electrochemical reactions occur on this surface. The amount of electrolyte used in each cell was 30 μL. The sulfur weight contained in each cell was ca. 1.92 mg, and the E/S ratio was ca. 15.6 mL g^{-1}. The assembled coin cells were discharged in the galvanostatic mode at discharge currents ranging from 0.01C to 0.4C at room temperature with a cutoff voltage of 1.8 V using a Neware multichannel battery cycler. The EIS of the cells were measured on a frequency response analyzer (Gamry Instruments Reference 3000) with an ac voltage amplitude of 10 mV.

The morphologies of the electrodes were investigated by SEM using a JEOL-JSM7401F microscope and by atomic force microscopy (AFM) using a Bruker Dimension Icon microscope. The energy-dispersive spectroscopy (EDS) element mapping was performed using the same JEOL microscope at an accelerating voltage of 20 kV. To observe the morphology evolution of the cathode at different DODs and at different rates, the disassembled cathodes after discharge were washed with DOL solution five times to remove the soluble polysulfides and Li salt, and then left in the glovebox overnight to evaporate the remaining solvent. To observe the cross-sectional view, a thin slice was cut from the cathode and placed nearly vertically on the sample holder for SEM.

3. MATHEMATICAL MODEL

The model describes nucleation, growth, and surface passivation using the theory presented in ref 33, which is slightly modified in this work to account for the fact that the electrodes are flat and is simplified to describe a smaller number of species and electrochemical reactions. For simplicity, in this work we assume that the only electrochemical reactions in the cell are Li oxidation at the anode

$$\mathrm{Li} \leftrightarrow \mathrm{Li}^+ + \mathrm{e}^- \tag{1}$$

and sulfur reduction at the cathode

$$\mathrm{S_4}^{2-} + 6\mathrm{e}^- \leftrightarrow 4\mathrm{S}^{2-} \tag{2}$$

In addition to the above electrochemical reactions, we also consider Li_2S deposition at the cathode according to the following precipitation/dissolution reaction:

$$2\mathrm{Li}^+ + \mathrm{S}^{2-} \leftrightarrow \mathrm{Li_2S(s)} \tag{3}$$

The deposition of Li_2S includes the electrochemical reduction reaction at the electrolyte/carbon interface and the chemical precipitation reaction at the cathode, which we refer to as a dissolution−precipitation process. The detailed description of the transport model and the boundary conditions at anode and cathode can be found in Supporting Information.

The EIS spectra were computed using the technique presented in ref 35. We assumed a small-signal harmonic perturbation of the discharge current $\tilde{i}e^{j\omega t}$ where $\tilde{i}$ is the complex magnitude and ω is the angular frequency of the signal and computed the small-signal response of the cell voltage, $\tilde{v}e^{j\omega t}$, numerically. The complex impedance was then computed using

$$Z = \frac{\tilde{v}}{\tilde{i}} \tag{4}$$

The computation details and the numerical method that was developed to calculate the small-signal resistances and capacitances can be found in the Supporting Information.

DOI: 10.1021/acsaem.9b00524
ACS Appl. Energy Mater. 2019, 2, 3860−3868

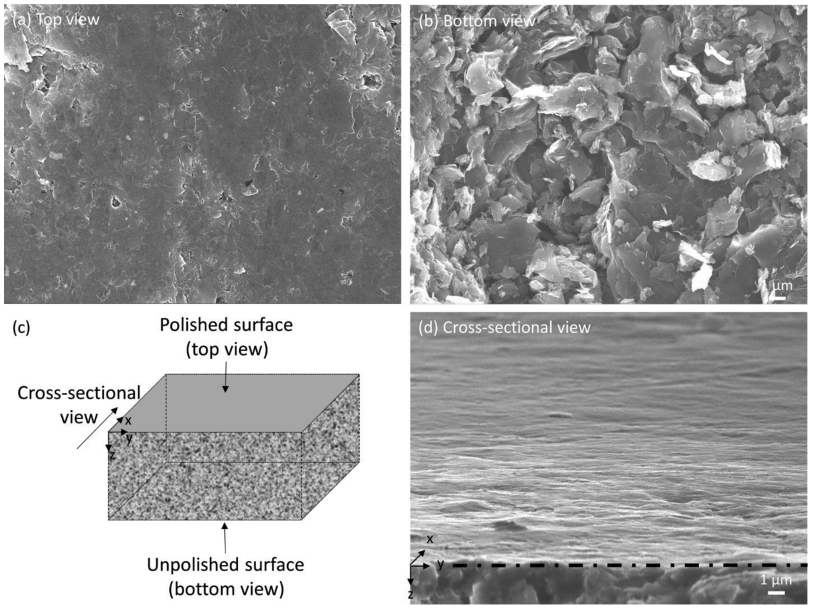

Figure 1. Morphology of pristine graphite cathode. (a) SEM image of the polished graphite surface. (b) SEM image of the unpolished graphite surface. (c) Schematic illustration of the graphite cathode. (d) Cross-sectional view of the graphite cathode.

4. RESULTS AND DISCUSSION

Figure 1 shows the morphology of the pristine graphite cathode. Figure 1a shows the SEM image of the polished graphite cathode. The AFM image of the polished graphite surface (see Figure S2 in Supporting Information) shows that the height variation of the surface is within ±200 nm. The calculated projected surface area (i.e., the integrated surface area of the topography in the scanned image area) is only 0.591% large than the scanned image area, indicating that the polished graphite surface has a near-2D flat morphology. In contrast, the unpolished graphite surface (see Figure 1b) exhibits a typical graphite morphology with numerous and rather irregular bulk particles/sheets in their shapes. The cross-sectional image of the graphite shows that the polished surface is relatively flat with marginal height variations compared to the pristine surface (see Figure 1c,d). Compared to the conventional porous composite materials for cathodes for Li−S batteries, the polished graphite exhibits a near-2D flat surface morphology, which provides an ideal substrate for direct visualization of Li_2S deposition in this study.

To simplify the electrochemical and chemical reactions involved in this study but also to avoid the possible deposition of high-order LiPS, in this work we used Li_2S_4 dissolved in electrolyte, as the starting material for the discharge reaction. In this way, the redox process can be simplified as the conversion between Li_2S_4 and Li_2S ($Li_2S_4 + 6Li \leftrightarrow 4Li_2S$), and more complex multistep liquid phase reactions occurring at the upper plateau of the voltage profile can be neglected.[36−38] The voltage profiles of the discharge curves at different rates are plotted in Figure 2 for the polished graphite cathode with Li_2S_4 catholyte. Disproportionation reactions can introduce a mixture of multiple polysulfide species in the electrolyte and therefore introduce a small portion of discharge capacity on the upper plateau.[39−41] However, as we can see from the discharge curve at low rate (0.01C), disproportionation reactions do not affect the total theoretical capacity of the Li−Li_2S_4 cell of 1254 mAh g^{-1}. As we increase the discharge

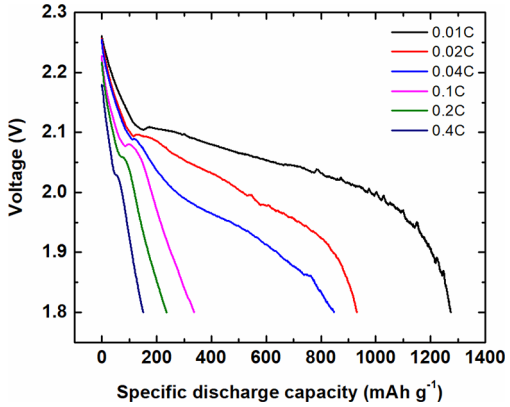

Figure 2. Discharge curves measured of Li−S cells with polished graphite cathode at different discharge currents.

current, the specific capacity decreases monotonously, while the polarization of the discharge curves increases considerably.

To analyze the morphology evolution of Li_2S during discharge, several Li−S cells were discharged to different DODs and at different rates. The corresponding cathodes were harvested after disassembly within 1 h upon the completion of the test to minimize the additional dissolution and precipitation of the deposit product during long periods of rest (although we have not observed a change in the morphology of the deposit product on our SEM images upon different durations of rest, it is still possible for the changes to occur). Their morphologies ware observed under SEM imaging, while the sulfur element mapping of the same area is analyzed using EDS. Figure 3 summarizes the combined SEM/EDS results. Since the cells were discharged by starting with a fresh liquid Li_2S_4 catholyte to avoid any possible LiPS precipitation[7,42] and the harvested cathodes were washed multiple times with DOL to dissolve any soluble species such as Li salt and LiPS, the solid product presented in the SEM images is expected to be solely Li_2S. We also conducted SEM on the Celgard separator after discharge and found a small

DOI: 10.1021/acsaem.9b00524
ACS Appl. Energy Mater. 2019, 2, 3860−3868

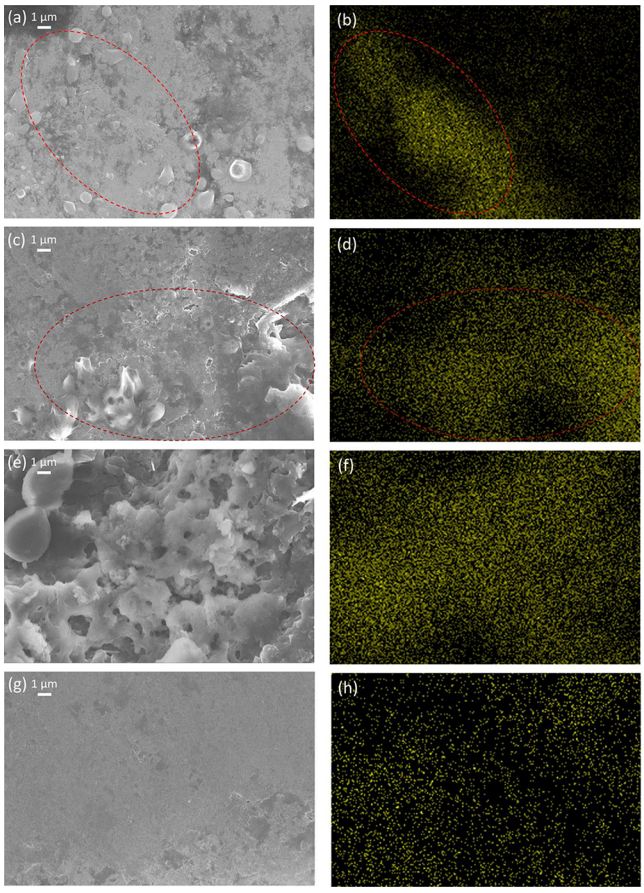

Figure 3. SEM and corresponding EDS mapping images of graphite cathodes at different DODs and discharge rates. (a, b) Surface view and sulfur mapping of the graphite cathode discharged to 33% DOD at 0.01C. (c, d) Surface view and sulfur mapping of the graphite cathode discharged to 67% DOD at 0.01C. (e, f) Surface view and sulfur mapping of the graphite cathode discharged to 100% DOD at 0.01C. (g, h) Surface view and sulfur mapping of the graphite cathode discharged to 67% DOD at 0.4C.

amount of solid product; however, the amount of the solid product was negligible compared to that deposited on the cathode surface (see Figure S3 in the Supporting Information). The EDS images show a relatively good correlation between the solid particle regions and sulfur element mapping (see the dashed regions in Figure 3a–d), also indicating the solid product is Li_2S. However, the EDS mapping exhibits a limited resolution toward a single particle shape but rather shows the intensity variation of Li_2S in the analyzed area. As seen in Figure 3a,b, when the graphite cathode was discharged to 33% DOD at 0.01C, a significant portion of the surface has been already covered by solid product. Meanwhile, some isolated Li_2S "islands" with nonuniform particle size can be observed. When the graphite cathode was further discharged to 67% DOD (see Figure 3c), most of these islands have coalesced together and separate solid particles were no longer observable. When the Li–S cell was fully discharged (100% DOD), we observed an extremely dense and porous deposition of Li_2S on the surface of graphite and the cathode exhibits a 3D morphology with a nonuniform distribution of the solid product (see Figure 3e). The intensity variation of sulfur element mapping in Figure 3f also indicates that the solid product has a nonuniform and irregular distribution. The combined results in Figure 3a–f suggest that Li_2S follows a dissolution–precipitation mechanism to gradually passivate the entire surface.

When the discharged current was switched from 0.01C to 0.4C, the morphology of Li_2S deposition is considerably different with no Li_2S islands distinguishable during the discharge process. Instead, the surface of the cathode presents a relatively smooth and 2D morphology along the whole discharge process, and in Figure 3g,h we present the SEM/EDS images of the fully discharged cathode at 0.4C. We can see that the cathode surface resembles its pristine morphology and sulfur mapping is relatively uniform in the analyzed area. The above result strongly supports the fact that the nucleation process is rate-dependent and the low discharge currents promote the growth of Li_2S in the direction perpendicular to

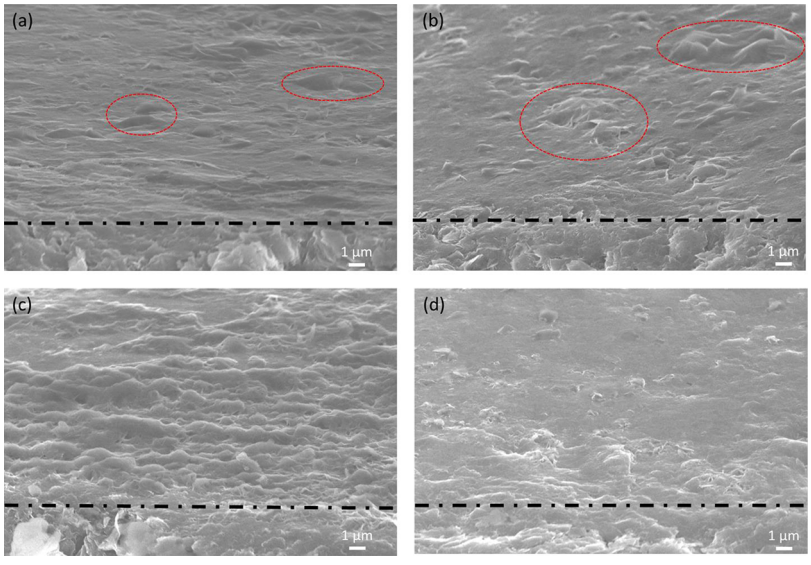

Figure 4. Cross-sectional SEM images of graphite cathodes at different DODs and rates. (a) SEM image of graphite cathode discharged to 33% DOD at 0.01C. (b) SEM image of graphite cathode discharged to 66% DOD at 0.01C. (c) SEM image of graphite cathode discharged to 100% DOD at 0.01C. (d) SEM image of graphite cathode discharged to 100% DOD at 0.4C.

DOI: 10.1021/acsaem.9b00524
ACS Appl. Energy Mater. 2019, 2, 3860–3868

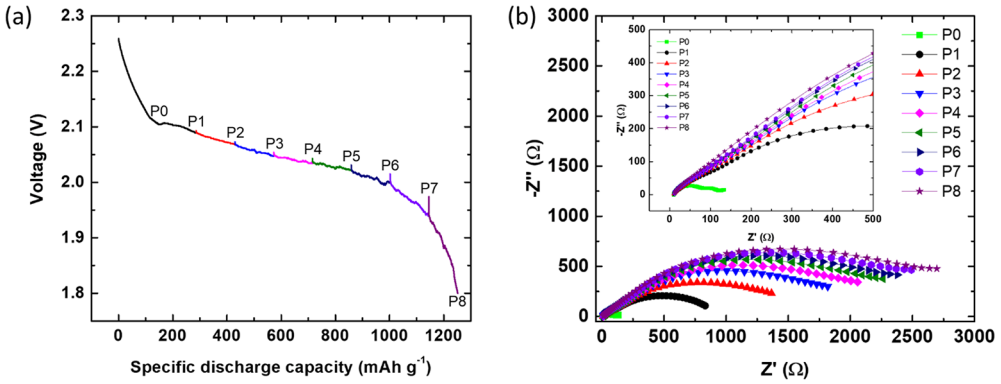

Figure 5. In situ EIS spectra of Li−S cell with graphite cathode at 0.01C. (a) Discharge voltage profile of Li−S cell with graphite cathode at 0.01C. (b) EIS spectra of Li−S cell discharged to different DODs.

the surface of the cathode, resulting in the formation of large 3D particles on this surface.

The cross-sectional images in Figure 4 further describe the growth process of Li_2S from a macroscopic view. As seen in Figure 4a, when the cell was discharged to 33% DOD at 0.01C, the flat surface starts to exhibit some variation in height (see the red circles), corresponding to the nonuniform nucleation and precipitation of Li_2S. As the discharge continued, the height/thickness of Li_2S islands has significantly increased to micrometer dimensions (see Figure 4b). When the cell was fully discharged, the variation of the thickness for the Li_2S layer is clearly observed as seen in Figure 4c. In contrast, for the cathode discharged at the increased rate there is little thickness variation for the Li_2S layer in the cross-sectional view in Figure 4d, consistent with the results in Figure 3g,h. The above results indicate again that the cathode discharged at high rates exhibits a relatively 2D thin-film-like morphology instead of the 3D morphology observed at low discharge rates. Due to the low discharge capacity at high discharge rates, the volume density of the final solid product is much smaller in the case of the cathode discharged at 0.4C than in the case of the cathode discharged at 0.01C. To compare the morphology obtained after the deposition of the same amount of Li_2S (i.e., similar capacity in lower plateau), we have tracked the cathode morphology at an early stage of discharge (<33% DOD) for the cathode discharged at 0.01C. We observed that at this stage the discharge product consistently exhibits the "islands" shape morphology, which is not observed at high discharge rates. This fact suggests that the discharge current plays a major effect in the morphology of the solid product in our cells.

A detailed mathematical analysis of the rate-dependent characteristics of the discharge curves is presented in ref 33. The rate at which the nuclei appear on the surface of the cathode depends on the rate of the electrochemical reactions and, hence, on the discharge rate of the battery. At low discharge rates the number of nuclei formed per unit time and unit area of the cathode is smaller than in the case of high discharge rate. Although smaller in number, the nuclei grow relatively large during the discharge on the lower plateau, forming large agglomerates of Li_2S (as the Li_2S "islands" in the above SEM images). At large discharge currents the number of nuclei formed per unit time and unit area is larger, resulting in a high density of nucleation seeds on the surface of the cathode. This large number of nucleation seeds passivates the surface of the cathode relatively fast and interrupts the electrochemical reactions, which results in a decrease of the specific capacity of the cell. Consequently, the Li_2S particle size is relatively small, and the deposition is more uniform on the surface (see Figure 3g,h). Next, we focus mostly on understanding the surface passivation effects on EIS at low discharge rates with combined experimental and theoretical approach.

EIS is often utilized as a powerful diagnostic tool for investigating the physical and chemical processes occurring at the electrode/electrolyte interfaces during discharge and charge.[40,43] In the literature, however, the conclusions drawn by analyzing the features of the spectra are not consistent, and sometimes even incorrect. There are a couple of reasons that account for the difficulty in analyzing the EIS data. First, the dissolution of the sulfur and formation of the intermediate LiPS products in the electrolyte can trigger significant redox shuttle effects. Its complexity and time dependence make the separation of the impedance contributions from different components of the batteries extremely challenging. Second, recent studies[44] show that the total cell impedance of Li−S batteries with high cathode area is dominated by the lithium anode rather than the cathode because the cathode area is much higher than anode area (also see Figure S4 in Supporting Information). However, due to the extremely low active surface area of graphite cathode used in our study and because the surface of the cathode is covered progressively by insulating Li_2S, the cathode dominates the total impedance of the cell. Consequently, the measured EIS directly reflect the increase of the kinetic resistance due to surface coverage effects by Li_2S. As seen in the in situ EIS curves measured during the low rate discharge process in Figure 5, the impedance generally has a rather nonlinear increasing trend along with DOD, which again indicates that the growth of Li_2S does not follow a thin-film-like lateral growth mechanism. Also note that point P1 belongs to the upper plateau, where no Li_2S precipitation had occurred. The corresponding EIS curve consists of two semicircles (see the inset of Figure 5b), which can be attributed to the cathode and anode impedance, respectively. Starting from P2 where the deposition of Li_2S took place, the EIS curves gradually become one semicircle, which indicates that, from this moment on, the cathode impedance dominates the total impedance of the battery. One can also see that the rate at which the resistance increases is significantly higher at the beginning of the solid product deposition (from P1 to P2) and decreases with the DOD. Therefore, the surface coverage is a nonlinear process, and at the beginning of the lower plateau a significant portion of the cathode is being passivated

DOI: 10.1021/acsaem.9b00524
ACS Appl. Energy Mater. 2019, 2, 3860−3868

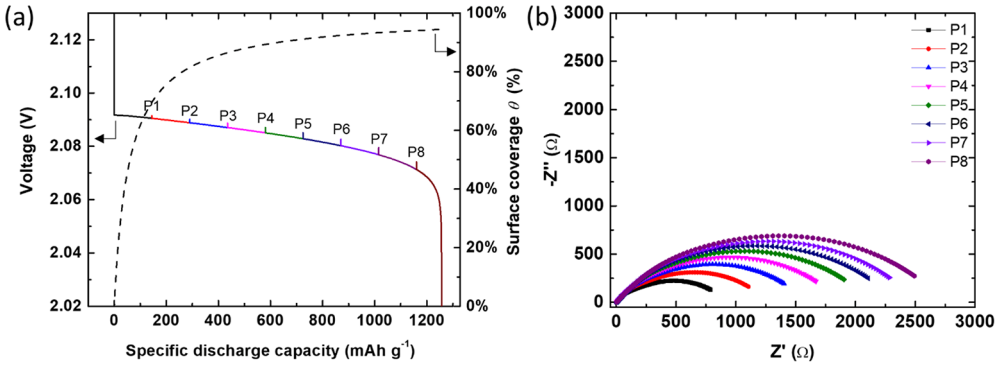

Figure 6. Simulated voltage profile and EIS spectra of Li−S cell with graphite cathode at 0.01C. (a) Discharge voltage profile of Li−S cell with graphite cathode at 0.01C. (b) Simulated EIS spectra of Li−S cell discharged to different DODs.

with Li_2S. Also note that the impedance semicircles on the Nyquist plot are depressed and the degree of depression of the EIS does not depend on the DOD.

Figure 6a shows the simulated voltage characteristic of the Li−S cell with a polished graphite cathode at 0.01C using the model described in Section 3. One can see that the simulated voltage has zero capacity contribution from the upper plateau due to the fact that the complex disproportionation reactions are not considered in the model and, therefore, the simulated discharge curve accounts only for the oversaturation of the electrolyte[33,45] and the subsequent solid deposition processes. In addition, the evolution of surface coverage θ, which is a measure of how much the cathode area is passivated with discharge product, is plotted as a function of the discharge capacity using a dashed line in Figure 6a. In agreement with our previous results[33] and the discussion in the Experimental Section, the surface coverage does not vary linearly during the solid deposition but increases faster at the beginning of the discharge compared to the end of the discharge. This phenomenon is due to the fact that the Li_2S seeds are initially small and the rate at which the surface coverage of these seeds increases is much larger at the beginning of the discharge than at the end of the discharge (see Figure S1 in Supporting Information). Therefore, most of the electrochemically active surface of the cathode is being passivated at the beginning of the discharge. When the cell dies, because of the low discharge rate, the surface coverage is close to but less than 100%, indicating that the cathode surface was not fully passivated by the time the active material is consumed. However, at increased discharge rates, the surface passivation will become a major obstacle to achieve high discharge capacity.[33]

To the best of our knowledge, the simulation of the impedance response of Li−S cells using physics-based models was only occasionally reported in the literature and no detailed discussion was provided.[46] The major advantage of using the physics-based model presented in Supporting Information to describe the discharge of the battery is that the impedance curves can be easily calculated and the origin of the different features on the Nyquist plots can be understood. Unlike in circuit-based models that are often employed to merely fit the impedance measurements to a number of parameters, by using a physics-based model to simulate the impedance curves one can relate the observed features of the impedance spectra to the particular electrochemical processes in the battery without preassuming any origins of the impedance. The simulated EIS curves are presented in Figure 6b. These curves agree qualitatively well with the experimental data presented in Figure 5. The resistance increase during discharge exhibits a rather nonlinear behavior trend due to the nonlinear nature of the surface coverage condition. In addition to the surface coverage, the variation of electron conductivity and Li ion transport during discharge could also affect the morphology of deposition and contribute to the nonlinear increment of the total impedance.

The mathematical model presented in the Supporting Information allows us to compute the values of the small-signal resistances and capacitances that appear in equivalent circuit diagrams of Nyquist plots. Traditionally, these diagrams are derived by fitting the EIS to circuit diagrams; however, in this work they are derived directly from the model equations. The results of this computation are presented in Figure 7,

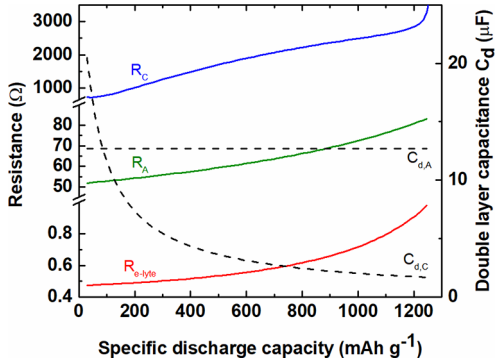

Figure 7. Simulated charge-transfer resistance at the anode (R_A) and cathode (R_C), small-signal resistance of the electrolyte ($R_{e\text{-}lyte}$), and double layer capacitance of the anode ($C_{d,A}$) and cathode ($C_{d,C}$). The values of the resistances and capacitances were computed by solving the finite element model presented in the Mathematical Model section.

which presents a few commonly used equivalent circuit components as a function of the DOD. In qualitative agreement with the experimental measurements, our simulations show that the cathode resistance increases from approximately 850 to over 3 kΩ because of surface passivation; the anode resistance increases from approximately 52 to 83 Ω because of the variation of the Li ion concentration during discharge, and the electrolyte resistance increases from approximately 0.5 to 1 Ω because of the decrease of the ion concentration during discharge. It is important to note that our model allows one to compute the values of the components in the equivalent circuit diagram even in the case when some of

DOI: 10.1021/acsaem.9b00524
ACS Appl. Energy Mater. 2019, 2, 3860−3868

these values are hard to determine experimentally. For instance, since R_A is much smaller than R_C and the two semicircles on the Nyquist plot overlap, it is hard if not impossible to determine resistance R_A by fitting the experimental EIS to equivalent circuits. In addition, our model offers a simple way to estimate the surface coverage θ, as a function of the DOD experimentally. Indeed, since the charge-transfer resistance at the cathode is inversely proportional to the active area of the cathode, we have $1 - \theta \approx \frac{R_{C,0}}{R_C}$, where $R_{C,0}$ is the charge-transfer resistance at the beginning of the nucleation process. This equation can be used to compute the surface coverage in Li−S batteries, by simply determining the charge-transfer resistance of the cathode as a function of DOD from EIS.

It needs to be pointed out that although the currents applied in the study are relatively small, the calculated current density per surface area of the graphite cathode is considerably higher than that in a porous high-surface-area cathode (see Supporting Information). Therefore, our results suggest the possibility of obtaining a high specific capacity even with low-surface-area cathodes, which was also confirmed by other research groups.[26,27,47] This is due to the fact that the achievable discharge capacity in the lower plateau is determined by how fast the surface area is covered rather than by how large the initial surface area of the cathode is. Cathodes with large specific areas have small current densities, which enhance their rate capability; however, their active area is covered very fast at the beginning of the lower plateau, resulting in discharge capacities similar to those of cathodes with reduced specific area at low discharge rates.

From a practical point of view, the use of nonporous cathodes is indeed more favorable to reduce the unfavorable side reactions between cathode and electrolyte that result in the formation of cathode electrolyte interphase.[48] For high-loading cathodes of Li−S batteries, the cell operation at low E/S ratios is extremely challenging partially because of the continuous electrolyte consumption over long-term cycles. Nonporous cathodes can minimize the electrolyte consumption at the cathode side and, thus, allow a decrease in the E/S ratio at no cost of sacrificing the electrochemical stability. However, in literature studies, cathode materials with high surface areas are dominantly employed. In Figure 8, we calculate the average Li_2S thickness of various Li−S batteries in recent papers (see Supporting Information for details). For most reported cathodes, the average Li_2S thickness is about or less than 10 nm after discharge. A higher thickness close to 100 nm is achieved only when a low-surface-area cathode is utilized and when the Li_2S deposition is well-regulated to promote the longitude growth. Our work provides a clear demonstration of Li_2S deposition in micrometer size and indicates the potential for using nonporous cathodes with moderate surface areas to achieve a high discharge capacity in Li−S batteries. For instance, a hierarchical cathode with macropores on a micrometer scale combined with balanced mesopores may prove to be a rational configuration to improve the discharge capacity at a cell level. We also notice that there are very limited reports of nonporous cathodes that operated at a relatively high discharge rate (e.g., above 1C), which poses another challenge for practical application. The cathode surface area should be therefore carefully designed to enable the cell operation at low E/S ratios and under realistic current densities.

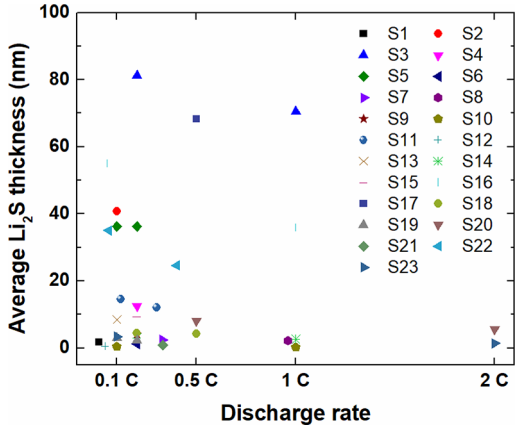

Figure 8. Calculated average Li_2S thickness of various Li−S batteries in the literature.

In addition, the proposed surface passivation mathematical model used in this article can also be applied to other types of battery chemistries. For instance, it can be applied to describe surface coverage effects by Li_2O_2 in Li−air batteries[49] and by Na_2S_2/Na_2S in room-temperature Na−S batteries.[50] These batteries encounter similar technical challenges caused by surface passivation during cell operation, and their solid deposition mechanism can be investigated in a similar manner.

The precipitation of Li_2S plays an important role in the performance of Li−S batteries. It is generally accepted that the cathode morphology can change during cycling, which greatly affects the cycle performance in the long-term operation.[51] Moreover, as indicated by Pan et al.[18] and Kleain et al.,[52] the insulating nature of Li_2S can inhibit its full dissolution during charge and it is likely that there is a maximum thickness of Li_2S layer that can be recharged and fully utilized under realistic operation conditions. Consequently, understanding the deposition mechanism is pivotal to ensure the rechargeability of the batteries. The understanding and controlling of the Li_2S redissolution and sulfur redeposition process during charge is a possible future avenue of study that deserves more research efforts.[53]

5. CONCLUSION

In this work, we have analyzed the precipitation mechanism of Li_2S during the lower plateau of discharge of Li−S batteries. A polished graphite cathode was utilized as the standard cathode material in an effort to obtain a more complete understanding of the growth process of Li_2S. The morphology of the discharge product depends on the DODs and discharge rate of the battery. At the end of the discharge and at low discharge rates, Li_2S particles with dimensions of over 1 μm are observed on the near-2D flat graphite surface. The dependence of the morphology on the discharge rate and the in situ EIS strongly support the assumption that the Li_2S follows a dissolution−precipitation mechanism during discharge. Furthermore, the presented experimental observations were verified using a new mathematical model for Li−S batteries. The model describes the cathode surface coverage process during discharge and predicts the experimental EIS spectra quantitatively well. This work is expected to provide insight for developing efficient strategies to defer cathode surface passivation in Li−S batteries. Our results also indicate the potential utilization of nonporous carbons as alternative sulfur hosts in Li−S batteries

DOI: 10.1021/acsaem.9b00524
ACS Appl. Energy Mater. 2019, 2, 3860−3868

to balance between the electrochemical performance and necessary cell parameters for practical Li−S batteries.

■ ASSOCIATED CONTENT

Supporting Information

The Supporting Information is available free of charge on the ACS Publications website at DOI: 10.1021/acsaem.9b00524.

Detailed description of the mathematical model, AFM image of polished graphite surface and SEM image of Celgard separator, EIS spectra of a cycled Li−S cell with a porous CNT foam cathode, calculation of surface area specific current density of the graphite cathode and a porous CNT cathode, and calculation of average Li_2S thickness from literature studies (PDF)

■ AUTHOR INFORMATION

Corresponding Author

*E-mail: zheng@eng.famu.fsu.edu.

ORCID

Chao Shen: 0000-0001-5270-4841

Jim P. Zheng: 0000-0003-2689-0067

Author Contributions

The manuscript was written through contributions of all authors. All authors have given approval to the final version of the manuscript.

Notes

The authors declare no competing financial interest.

■ ACKNOWLEDGMENTS

We thank Dr. Eric Lochner for taking the AFM image of graphite. The work is supported by NSF Grants 1609860 and 1805288.

■ REFERENCES

(1) Nitta, N.; Wu, F.; Lee, J. T.; Yushin, G. Li-Ion Battery Materials: Present and Future. *Mater. Today* **2015**, *18* (5), 252−264.

(2) Chung, S. H.; Chang, C. H.; Manthiram, A. Progress on the Critical Parameters for Lithium−Sulfur Batteries to Be Practically Viable. *Adv. Funct. Mater.* **2018**, *28* (28), 1801188.

(3) Li, S.; Jin, B.; Zhai, X.; Li, H.; Jiang, Q. Review of Carbon Materials for Lithium-Sulfur Batteries. *Chemistry Select.* **2018**, *3* (8), 2245−2260.

(4) Xu, R.; Belharouak, I.; Zhang, X.; Chamoun, R.; Yu, C.; Ren, Y.; Nie, A.; Shahbazian-Yassar, R.; Lu, J.; Li, J. C. M.; et al. Insight into Sulfur Reactions in Li-S Batteries. *ACS Appl. Mater. Interfaces* **2014**, *6* (24), 21938−21945.

(5) Pan, H.; Han, K. S.; Vijayakumar, M.; Xiao, J.; Cao, R.; Chen, J.; Zhang, J.; Mueller, K. T.; Shao, Y.; Liu, J. Ammonium Additives to Dissolve Lithium Sulfide through Hydrogen Binding for High-Energy Lithium-Sulfur Batteries. *ACS Appl. Mater. Interfaces* **2017**, *9* (5), 4290−4295.

(6) Fang, R.; Zhao, S.; Sun, Z.; Wang, D. W.; Cheng, H. M.; Li, F. More Reliable Lithium-Sulfur Batteries: Status, Solutions and Prospects. *Adv. Mater.* **2017**, *29* (48), 1606823.

(7) Shen, C.; Xie, J.; Zhang, M.; Andrei, P.; Hendrickson, M.; Plichta, E. J.; Zheng, J. P. Understanding the Role of Lithium Polysulfide Solubility in Limiting Lithium-Sulfur Cell Capacity. *Electrochim. Acta* **2017**, *248*, 90−97.

(8) Shen, C.; Xie, J.; Zhang, M.; Andrei, P.; Hendrickson, M.; Plichta, E. J.; Zheng, J. P. Self-Discharge Behavior of Lithium-Sulfur Batteries at Different Electrolyte/Sulfur Ratios. *J. Electrochem. Soc.* **2019**, *166* (3), A5287−A5294.

(9) Manthiram, A.; Fu, Y.; Chung, S.; Zu, C.; Su, Y. Rechargeable Lithium−Sulfur Batteries. *Chem. Rev.* **2014**, *114* (23), 11751−11787.

(10) Zhang, G.; Zhang, Z.-W.; Peng, H.-J.; Huang, J.-Q.; Zhang, Q. A Toolbox for Lithium-Sulfur Battery Research: Methods and Protocols. *Small Methods.* **2017**, *1* (7), 1700134.

(11) Feng, S.; Zhong, H.; Song, J.; Zhu, C.; Dong, P.; Shi, Q.; et al. Catalytic Activity of Co-X (X = S, P, O) and Its Dependency on Nanostructure/Chemical Composition in Lithium-Sulfur Batteries. *ACS Appl. Energy Mater.* **2018**, *1*, 7014−7021.

(12) Wang, T.; Yang, Y.; Fan, L.; Wang, L.; Ma, R.; Zhang, Q.; Zhao, J.; Ge, J.; Lu, X.; Yu, X.; et al. Ultrathin Honeycomb-like Carbon as Sulfur Host Cathode for High Performance Lithium-Sulfur Batteries. *ACS Appl. Energy Mater.* **2018**, *1*, 7076.

(13) Gao, T.; Yu, Z.; Huang, Z.-H.; Yang, Y. Nitrogen/Oxygen Dual-Doped Carbon Nanofibers as an Electrocatalytic Interlayer for a High Sulfur Content Lithium−Sulfur Battery. *ACS Appl. Energy Mater.* **2019**, *2* (1), 777−787.

(14) Guo, J.; Zhao, S.; He, G.; Zhang, F. Novel Synergistic Strategy for Developing High-Performance Lithium Sulfur Batteries of Large Areal Sulfur Loading by SEI Modified Separator. *ACS Appl. Energy Mater.* **2018**, *1* (3), 932−940.

(15) Meng, Z.; Zhang, S.; Wang, J.; Yan, X.; Ying, H.; Xu, X.; Zhang, W.; Hou, X.; Han, W.-Q. Nickel-Based-Hydroxide-Wrapped Activated Carbon Cloth/Sulfur Composite with Tree-Bark-Like Structure for High-Performance Freestanding Sulfur Cathode. *ACS Appl. Energy Mater.* **2018**, *1*, 1594.

(16) Yang, Y.; Zheng, G.; Misra, S.; Nelson, J.; Toney, M. F.; Cui, Y. High-Capacity Micrometer-Sized Li 2S Particles as Cathode Materials for Advanced Rechargeable Lithium-Ion Batteries. *J. Am. Chem. Soc.* **2012**, *134* (37), 15387−15394.

(17) Kolosnitsyn, V. S.; Kuzmina, E. V.; Karaseva, E. V. On the Reasons for Low Sulphur Utilization in the Lithium-Sulphur Batteries. *J. Power Sources* **2015**, *274*, 203−210.

(18) Pan, H.; Han, K. S.; Engelhard, M. H.; Cao, R.; Chen, J.; Zhang, J.-G.; Mueller, K. T.; Shao, Y.; Liu, J. Addressing Passivation in Lithium-Sulfur Battery Under Lean Electrolyte Condition. *Adv. Funct. Mater.* **2018**, *28*, 1707234.

(19) Yan, J.; Liu, X.; Li, B. Capacity Fade Analysis of Sulfur Cathodes in Lithium-Sulfur Batteries. *Adv. Sci.* **2016**, *3* (12), 1600101.

(20) Demir-Cakan, R. Targeting the Role of Lithium Sulphide Formation for the Rapid Capacity Fading in Lithium-Sulphur Batteries. *J. Power Sources* **2015**, *282*, 437−443.

(21) Ryu, H. S.; Guo, Z.; Ahn, H. J.; Cho, G. B.; Liu, H. Investigation of Discharge Reaction Mechanism of Lithiumlliquid Electrolytelsulfur Battery. *J. Power Sources* **2009**, *189* (2), 1179−1183.

(22) Fan, F. Y.; Carter, W. C.; Chiang, Y.-M. Mechanism and Kinetics of Li $_2$ S Precipitation in Lithium-Sulfur Batteries. *Adv. Mater.* **2015**, *27* (35), 5203−5209.

(23) Ren, Y. X.; Zhao, T. S.; Liu, M.; Tan, P.; Zeng, Y. K. Modeling of Lithium-Sulfur Batteries Incorporating the Effect of Li2S Precipitation. *J. Power Sources* **2016**, *336*, 115−125.

(24) Gerber, L. C. H. H.; Frischmann, P. D.; Fan, F. Y.; Doris, S. E.; Qu, X.; Scheuermann, A. M.; Persson, K.; Chiang, Y. M.; Helms, B. A. Three-Dimensional Growth of Li2S in Lithium-Sulfur Batteries Promoted by a Redox Mediator. *Nano Lett.* **2016**, *16* (1), 549−554.

(25) Peng, H. J.; Zhang, G.; Chen, X.; Zhang, Z. W.; Xu, W. T.; Huang, J. Q.; Zhang, Q. Enhanced Electrochemical Kinetics on Conductive Polar Mediators for Lithium−Sulfur Batteries. *Angew. Chem., Int. Ed.* **2016**, *55* (42), 12990−12995.

(26) Yun, J. H.; Kim, J. H.; Kim, D. K.; Lee, H. W. Suppressing Polysulfide Dissolution via Cohesive Forces by Interwoven Carbon Nanofibers for High-Areal-Capacity Lithium-Sulfur Batteries. *Nano Lett.* **2018**, *18* (1), 475−481.

(27) Pan, H.; Chen, J.; Cao, R.; Murugesan, V.; Rajput, N. N.; Han, K. S.; Persson, K.; Estevez, L.; Engelhard, M. H.; Zhang, J.-G.; et al. Non-Encapsulation Approach for High-Performance Li−S Batteries through Controlled Nucleation and Growth. *Nat. Energy.* **2017**, *2* (10), 813−820.

(28) Li, Z.; Zhou, Y.; Wang, Y.; Lu, Y.-C. Solvent-Mediated Li 2 S Electrodeposition: A Critical Manipulator in Lithium-Sulfur Batteries. *Adv. Energy Mater.* **2019**, *9* (1), 1802207.

DOI: 10.1021/acsaem.9b00524
ACS Appl. Energy Mater. 2019, 2, 3860−3868

(29) Lang, S. Y.; Xiao, R. J.; Gu, L.; Guo, Y. G.; Wen, R.; Wan, L. J. Interfacial Mechanism in Lithium-Sulfur Batteries: How Salts Mediate the Structure Evolution and Dynamics. *J. Am. Chem. Soc.* **2018**, *140* (26), 8147−8155.
(30) Chu, H.; Noh, H.; Kim, Y.-J.; Yuk, S.; Lee, J.-H.; Lee, J.; Kwack, H.; Kim, Y.; Yang, D.-K.; Kim, H.-T. Achieving Three-Dimensional Lithium Sulfide Growth in Lithium-Sulfur Batteries Using High-Donor-Number Anions. *Nat. Commun.* **2019**, *10* (1), 188.
(31) Ren, Y. X.; Zhao, T. S.; Liu, M.; Wei, L.; Zhang, R. H. High-Performance Nitrogen-Doped Titania Nanowire Decorated Carbon Cloth Electrode for Lithium-Polysulfide Batteries. *Electrochim. Acta* **2017**, *242*, 137−145.
(32) Liu, Z.; Mukherjee, P. P. Mesoscale Elucidation of Surface Passivation in the Li-Sulfur Battery Cathode. *ACS Appl. Mater. Interfaces* **2017**, *9* (6), 5263−5271.
(33) Andrei, P.; Shen, C.; Zheng, J. P. Theoretical and Experimental Analysis of Precipitation and Solubility Effects in Lithium-Sulfur Batteries. *Electrochim. Acta* **2018**, *284*, 469−484.
(34) Zhang, T.; Marinescu, M.; Walus, S.; Kovacik, P.; Offer, G. J. What Limits the Rate Capability of Li-S Batteries during Discharge: Charge Transfer or Mass Transfer? *J. Electrochem. Soc.* **2018**, *165* (1), A6001−A6004.
(35) Mehta, M.; Zhu, C.; Andrei, P. Statistical Analysis of Li-Oxygen Batteries. *ECS Trans.* **2017**, *75* (22), 35−45.
(36) Zheng, D.; Liu, D.; Harris, J. B.; Ding, T.; Si, J.; Andrew, S.; Qu, D.; Yang, X. Q.; Qu, D. Investigation of the Li-S Battery Mechanism by Real-Time Monitoring of the Changes of Sulfur and Polysulfide Species during the Discharge and Charge. *ACS Appl. Mater. Interfaces* **2017**, *9* (5), 4326−4332.
(37) Wu, H. L.; Huff, L. A.; Gewirth, A. A. In Situ Raman Spectroscopy of Sulfur Speciation in Lithium-Sulfur Batteries. *ACS Appl. Mater. Interfaces* **2015**, *7* (3), 1709−1719.
(38) Shen, C.; Xie, J.; Zhang, M.; Andrei, P.; Zheng, J. P.; Hendrickson, M.; Plichta, E. J. A Li-Li2S4 Battery with Improved Discharge Capacity and Cycle Life at Low Electrolyte/Sulfur Ratios. *J. Power Sources* **2019**, *414* (October), 412−419.
(39) Wild, M.; O'Neill, L.; Zhang, T.; Purkayastha, R.; Minton, G.; Marinescu, M.; Offer, G. J. Lithium Sulfur Batteries, a Mechanistic Review. *Energy Environ. Sci.* **2015**, *8* (12), 3477−3494.
(40) Drvarič Talian, S.; Moškon, J.; Dominko, R.; Gaberšček, M. Reactivity and Diffusivity of Li Polysulfides: A Fundamental Study Using Impedance Spectroscopy. *ACS Appl. Mater. Interfaces* **2017**, *9* (35), 29760−29770.
(41) Chung, S. H.; Han, P.; Manthiram, A. A Polysulfide-Trapping Interface for Electrochemically Stable Sulfur Cathode Development. *ACS Appl. Mater. Interfaces* **2016**, *8* (7), 4709−4717.
(42) Shen, C.; Xie, J.; Zhang, M.; Zheng, J. P.; Hendrickson, M.; Plichta, E. J. Communication—Effect of Lithium Polysulfide Solubility on Capacity of Lithium-Sulfur Cells. *J. Electrochem. Soc.* **2017**, *164* (6), A1220−A1222.
(43) Conder, J.; Villevieille, C.; Trabesinger, S.; Novák, P.; Gubler, L.; Bouchet, R. Electrochemical Impedance Spectroscopy of a Li−S Battery: Part 1. Influence of the Electrode and Electrolyte Compositions on the Impedance of Symmetric Cells. *Electrochim. Acta* **2017**, *244*, 61−68.
(44) Wang, H.; Adams, B. D.; Pan, H.; Zhang, L.; Han, K. S.; Estevez, L.; Lu, D.; Jia, H.; Feng, J.; Guo, J.; et al. Tailored Reaction Route by Micropore Confinement for Li-S Batteries Operating under Lean Electrolyte Conditions. *Adv. Energy Mater.* **2018**, *8*, 1800590.
(45) Kumaresan, K.; Mikhaylik, Y.; White, R. E. A Mathematical Model for a Lithium−Sulfur Cell. *J. Electrochem. Soc.* **2008**, *155* (8), A576.
(46) Fronczek, D. N.; Bessler, W. G. Insight into Lithium-Sulfur Batteries: Elementary Kinetic Modeling and Impedance Simulation. *J. Power Sources* **2013**, *244*, 183−188.
(47) Yu, R.; Chung, S. H.; Chen, C. H.; Manthiram, A. An Ant-Nest-like Cathode Substrate for Lithium-Sulfur Batteries with Practical Cell Fabrication Parameters. *Energy Storage Mater.* **2019**, *18* (November), 491.
(48) Ye, Y.; Song, M.-K.; Xu, Y.; Nie, K.; Liu, Y.; Feng, J.; Sun, X.; Cairns, E. J.; Zhang, Y.; Guo, J. Lithium Nitrate: A Double-Edged Sword in the Rechargeable Lithium-Sulfur Cell. *Energy Storage Mater.* **2019**, *16*, 498−504.
(49) Shen, C.; Xie, J.; Liu, T.; Zhang, M.; Andrei, P.; Dong, L.; Hendrickson, M.; Plichta, E. J.; Zheng, J. P. Influence of Pore Size on Discharge Capacity in Li-Air Batteries with Hierarchically Macroporous Carbon Nanotube Foams as Cathodes. *J. Electrochem. Soc.* **2018**, *165* (11), A2833−A2839.
(50) Ryu, H.; Kim, T.; Kim, K.; Ahn, J. H.; Nam, T.; Wang, G.; Ahn, H. J. Discharge Reaction Mechanism of Room-Temperature Sodium-Sulfur Battery with Tetra Ethylene Glycol Dimethyl Ether Liquid Electrolyte. *J. Power Sources* **2011**, *196* (11), 5186−5190.
(51) Noh, H.; Song, J.; Park, J.-K.; Kim, H.-T. A New Insight on Capacity Fading of Lithium−sulfur Batteries: The Effect of Li 2 S Phase Structure. *J. Power Sources* **2015**, *293*, 329−335.
(52) Klein, M. J.; Veith, G. M.; Manthiram, A. Rational Design of Lithium-Sulfur Battery Cathodes Based on Experimentally Determined Maximum Active Material Thickness. *J. Am. Chem. Soc.* **2017**, *139* (27), 9229−9237.
(53) Tan, C.; Heenan, T. M. M.; Ziesche, R. F.; Daemi, S. R.; Hack, J.; Maier, M.; Marathe, S.; Rau, C.; Brett, D. J. L.; Shearing, P. R. Four-Dimensional Studies of Morphology Evolution in Lithium−Sulfur Batteries. *ACS Appl. Energy Mater.* **2018**, *1* (9), 5090−5100.

DOI: 10.1021/acsaem.9b00524
ACS Appl. Energy Mater. 2019, 2, 3860−3868